Signatures of chaos in the entanglement of two coupled quantum kicked tops

Paul A. Miller and Sarben Sarkar
Department of Physics, King's College London, Strand, London WC2R 2LS, United Kingdom
(Received 19 October 1998)

We investigate the rate at which two initially decoupled quantum kicked tops become entangled upon the introduction of an interaction between them. We find that the entanglement eventually increases linearly in time. Moreover, we find that the rate of this linear increase is itself a linear function of the sum of the positive Lyapunov exponents when averaged over initial points drawn from the classical distributions corresponding to the initial quantum product state. The entanglement measure that is used allows us to identify entanglement with sensitive dependence on initial conditions. [S1063-651X(99)07005-1]

PACS number(s): 05.45.Mt

I. INTRODUCTION

Some previous approaches to the subject of quantum chaos [1–4] have been concerned with the behavior of classically unstable and classically chaotic quantum systems after they are coupled to heat baths [5–11]. These heat baths have typically been modeled by an infinite collection of harmonic oscillators with definite spectral densities. The infinite number of extra degrees of freedom introduced and subsequently traced over are intended to model the influence of the rest of the Universe [12,13] on the system; energy lost will never return [14]. The hope is that the decohering effect of the environment will restore the classical-quantum correspondence which was under threat from classical chaos [6].

The price exacted for the restoration of this correspondence is an increase in the system entropy or, equivalently, loss of knowledge about the state of a system. This leads to an increase in entanglement in a very precise way. One particular model, that of an inverted harmonic oscillator, has been shown to be useful as a guide to physical intuition in this context. It has been shown [6,15] that for weak coupling to a heat bath, the von Neumann entropy of the reduced dynamics will eventually increase at a rate which is approximately equal to the classical quantity analagous to a Lyapunov exponent. However, in an analysis of the open quantum behavior of the *genuinely* chaotic kicked rotor [11] it was found that the von Neumann entropy of the reduced dynamics increases at a rate which is a *linear function* of the Lyapunov exponent averaged over the points which comprise the classical state analagous to an initial quantum coherent state in phase space. Thus, the intuition gleaned from the study of the inverted oscillator is valid despite its manifold deficiencies as a model of true classical chaos [15].

A natural question to ask at this stage, therefore, is the following: how ubiquitous a phenomenon is the linearity of entropy increase in time, with a rate determined by a measure of the underlying classical chaos? In particular, is a thermal bath with an infinite number of degrees of freedom essential or could a finite chaotic system act in the same way? To address this question we must first remind ourselves of the reasons for entropy increase in quantum systems. Entropy increase, or an increasing lack of knowledge about the state of the system, results from the coupling of the system to another system, evolving the two together using a joint Hamiltonian, and then tracing over the degrees of freedom which are of no interest to us. The resulting *reduced* density matrix is then used to calculate the von Neumann entropy. An increase of the entropy implies that the two coupled systems have become *entangled* by the time at which the entropy is calculated, i.e., quantum correlations have developed. It will be essential to define measures of entanglement which can then be compared to entropy increase.

We shall therefore consider the increase in entanglement with time of two coupled quantum systems, in particular two coupled quantum kicked tops. Recently at a *qualitative* level Furuya *et al.* [16] have recently taken a similar approach with a different choice of system. One of the reasons for our choice is that the single kicked top is a much studied and well known [4,17–22] model of classical and quantum chaos. Its quantum dynamics is that of a spin-j particle precessing about a fixed axis but which is also perturbed or ''kicked'' periodically in time. Moreover, the finite dimensionality of its Hilbert space, viz., $2j+1$, makes it a convenient system to study since it eliminates the need for a truncation of the Hilbert space.

This paper is organized as follows. In Sec. II we will discuss the measure of entanglement we have used here and the reasons for choosing it. We then proceed to define both the quantum and the classical dynamics of the coupled kicked tops in Sec. III. In Sec. IV we define the initial direct product states used in the quantum analysis and their classically analagous distributions. The results of our numerical investigations are presented in Sec. V and we conclude in Sec. VI.

II. ENTANGLEMENT MEASURES

We will now discuss a way of quantifying entanglement which will be crucial to the development. One measure of the entanglement in a state σ, $E(\sigma)$, is the ''distance'' from the state to the set, $\mathcal{D}$, of all disentangled states defined by Vedral *et al.* in Refs. [23–25]:

$$E(\sigma) := \min_{\rho \in \mathcal{D}} D(\sigma \| \rho), \tag{1}$$

where $D(\sigma\|\rho)$ is *any* measure of the distance (not necessarily a metric) between the states σ and ρ such that some reasonable conditions are satisfied by $E(\sigma)$. There are a

number of advantages to this definition [23]. First, it is constructed especially in order to distinguish between quantum and classical correlations, being only nonzero for the former. Second, it is independent of the number of systems being considered. Finally, it is independent of the dimensionality of these systems. It is, therefore, a very general and useful definition of a measure of entanglement.

A natural question to ask, of course, is what, if any, distance measure $D(\sigma\|\rho)$ will enable the quantity $E(\sigma)$ of Eq. (1) to satisfy the given criteria and thereby render it a ''good'' measure of entanglement. Just such a suitable function was also proposed by Vedral *et al.* [23–25]; namely, the *quantum relative entropy* defined by

$$D(\sigma\|\rho)=S(\sigma\|\rho):=\mathrm{Tr}[\sigma(\ln\sigma-\ln\rho)]. \tag{2}$$

This definition, together with Eq. (1), defines a measure of entanglement known as the *relative entropy of entanglement*:

$$E(\sigma):=\min_{\rho\in\mathcal{D}}\mathrm{Tr}[\sigma(\ln\sigma-\ln\rho)]. \tag{3}$$

This also provides us with an *operational* interpretation of entanglement [23–25]: the greater the entanglement of a state σ, the fewer measurements on a separable state ρ it will take to prevent confusion with σ.

One more particularly important reason for restricting our attention to $E(\sigma)$ defined in Eq. (3) is the considerable simplification that arises in the case of pure states, σ. For pure entangled states the relative entropy of entanglement reduces to the von Neumann entropy of *either one* of the subsystems of the entangled pair [23]. Thus, when $\mathrm{Tr}\,\sigma^2=\mathrm{Tr}\,\sigma=1$, we have

$$E(\sigma)=-\mathrm{Tr}[\sigma_A\ln\sigma_A]=-\mathrm{Tr}[\sigma_B\ln\sigma_B], \tag{4}$$

where

$$\sigma_A:=\mathrm{Tr}_B[\sigma],\quad \sigma_B:=\mathrm{Tr}_A[\sigma]. \tag{5}$$

We will only consider pure states in this paper. This fact means that we need only calculate the (reduced) von Neumann entropy in order to determine the level of entanglement at any time. This amounts simply to a diagonalization of either one of the reduced density matrices. But the reduction of the measure of entanglement to the von Neumann entropy of either subsystem is also propitious in another way: we can now directly compare linear rates of entanglement increase — if, of course, they arise — with underlying measures of chaos in the hope that the relationship found will provide further evidence for the conjecture that classical instability begets quantum instability.

III. COUPLED KICKED TOPS

A. Quantum dynamics

Each kicked top is simply a spin-j particle with an angular momentum vector $\mathbf{J}_r\equiv(J_{x_r},J_{y_r},J_{z_r})$, $r=1,2$, the components of which obey the standard commutation relations. For example, $[J_{x_r},J_{y_r}]=iJ_{z_r}$ and $[\mathbf{J}_r^2,J_{z_r}]=0, r=1,2$, etc. However, the angular momentum operators of different tops also commute, e.g., $[J_{x_1},J_{y_2}]=0$, etc., and we can therefore choose the simultaneous eigenvectors of the set of four mutually commuting operators $\mathbf{J}_1^2,\mathbf{J}_2^2,J_{z_1}$, and J_{z_2} to be our choice of basis. We note that Planck's constant has been set to unity in the treatment that follows. The Hamiltonian of the coupled kicked tops can be now be written:

$$H(t)=H_1+H_2+H_I=\frac{\pi}{2}J_{y_1}+\frac{k}{2j}J_{z_1}^2\sum_{n=-\infty}^{\infty}\delta(t-n)+\frac{\pi}{2}J_{y_2}+\frac{k}{2j}J_{z_2}^2\sum_{n=-\infty}^{\infty}\delta(t-n)+\frac{k\varepsilon}{j}J_{z_1}J_{z_2}\sum_{n=-\infty}^{\infty}\delta(t-n). \tag{6}$$

The J_{y_r} terms describe the precession of each top around the y axis, each with an angular frequency of $\pi/2$. The remaining terms are due to a periodic δ-function ''kick.'' The first two such terms describe, respectively, impulsive nonlinear rotations or ''twists'' about each z axis, with each constant of proportionality being given by the dimensionless factor $k/2j$. The third and final such term describes the coupling between the tops using a spin-spin interaction term with a strength characterized by a dimensionless coupling constant $k\varepsilon/j$. Thus, the interaction is introduced as a consequence of the kick.

If we set the coupling constant, ε, equal to 0 in Eq. (6), then we will have a completely separable Hamiltonian describing the evolution of two noninteracting kicked tops. Let us examine the first of these tops. Its Hamiltonian is

$$H_1(t)=\frac{\pi}{2}J_{y_1}+\frac{k}{2j}J_{z_1}^2\sum_{n=-\infty}^{\infty}\delta(t-n), \tag{7}$$

and the commutation relations can be used to show $[\mathbf{J}_1^2,H_1(t)]=0$, also $[\mathbf{J}_1^2,J_{x_1}]=0$, and similarly for J_{y_1} and J_{z_1}. The basis vectors are then chosen as the eigenvectors of $\mathbf{J}_1^2$ and J_{z_1} [26] are denoted by $|j,m_1\rangle$ and obey

$$\mathbf{J}_1^2|j,m_1\rangle=j(j+1)|j,m_1\rangle, \tag{8}$$

$$J_{z_1}|j,m_1\rangle=m_1|j,m_1\rangle. \tag{9}$$

As j will be fixed in the following, we henceforth write $|m_1\rangle$ for $|j,m_1\rangle$. Both the classical and quantum features of the kicked top have been studied in some depth by various authors [4,19,20].

We will restrict our discussion to the $[(2j+1)\times(2j+1)]$-dimensional product space spanned by the eigenvectors of the operators $\mathbf{J}_1^2,\mathbf{J}_2^2,J_{z_1}$, and J_{z_2}. The basis kets can then be written $|j,m_1,j,m_2\rangle$ and are simply the tensor product of two single top basis kets, i.e.,

$$|j,m_1,j,m_2\rangle=|j,m_1\rangle\otimes|j,m_2\rangle. \tag{10}$$

In a similar shorthand to that used above, we henceforth write $|m_1,m_2\rangle$ for $|j,m_1,j,m_2\rangle$. They obey the eigenvalue equations

$$\mathbf{J}_1^2|m_1,m_2\rangle=j(j+1)|m_1,m_2\rangle, \tag{11}$$

$$\mathbf{J}_2^2|m_1,m_2\rangle = j(j+1)|m_1,m_2\rangle, \tag{12}$$

$$J_{z_1}|m_1,m_2\rangle = m_1|m_1,m_2\rangle, \tag{13}$$

$$J_{z_2}|m_1,m_2\rangle = m_2|m_1,m_2\rangle. \tag{14}$$

The unitary time evolution operator corresponding to the Hamiltonian of Eq. (6) is

$$U_{\text{tops}} = U_\varepsilon^{12}\, U^1\, U^2 = U_k^1\, U_k^2\, U_\varepsilon^{12}\, U_f^1\, U_f^2 \tag{15}$$

in which the various terms are given by

$$U^r := U_k^r\, U_f^r, \tag{16}$$

i.e., the evolution operator of a single kicked top,

$$U_k^r := \exp\left(-\frac{ik}{2j}J_{z_r}^2\right), \tag{17}$$

$$U_f^r := \exp\left(-\frac{i\pi}{2}J_{y_r}\right), \tag{18}$$

and

$$U_\varepsilon^{12} := \exp\left(-\frac{ik\varepsilon}{j}J_{z_1}J_{z_2}\right) \tag{19}$$

for $r=1,2$. It describes the free rotation of each top about its y axis followed by the introduction of the kick which gives each top a twist *and* couples them instantaneously. Note that the free evolution is assumed to have a negligible effect during the kick. The convenient separation of terms in Eq. (15) is a result of both the δ-function kick and the fact that operators corresponding to different tops commute.

In the Schrödinger picture the powers U_{tops}^n describe the evolution of an initial state of the system up to any one of the discrete sets of times $n=1,2,\ldots$. Thus

$$|\psi(n)\rangle = U_{\text{tops}}^n|\psi(0)\rangle, \tag{20}$$

where the initial state $|\psi(0)\rangle$ may already be an entangled state of the two tops. This is the method we will use to iterate our system in the numerical work that is discussed below.

B. Classical dynamics

We use the Heisenberg picture to determine the classical analog of our coupled top system. Now, of course, the operators change in time according to $\hat{A}(n+1) = U_{\text{tops}}^{-1}\hat{A}(n)U_{\text{tops}}$. We wish to determine the explicit form of the Heisenberg equations of motion for each of the six angular momentum operators of the system.

As an explicit example we will consider the time evolution of J_{x_1}. Using Eq. (15) we find

$$\begin{aligned} U_{\text{tops}}^{-1}J_{x_1}U_{\text{tops}} = {} & \frac{1}{2}(J_{z_1}+iJ_{y_1})\exp\left[\frac{ik}{j}\left(-J_{x_1}+\frac{1}{2}\right)\right] \\ & \otimes \exp\left(-\frac{ik\varepsilon}{j}J_{y_2}\right)+\frac{1}{2}(J_{z_1}-iJ_{y_1}) \\ & \times\exp\left[-\frac{ik}{j}\left(-J_{x_1}+\frac{1}{2}\right)\right]\otimes\exp\left(\frac{ik\varepsilon}{j}J_{y_2}\right). \end{aligned} \tag{21}$$

Similar equations hold for the other five angular momentum operators.

The introduction of a new set of rescaled angular momentum operators will facilitate the determination of the classical limit of our system. We define

$$\mathbf{X}_r \equiv (X_r,Y_r,Z_r) := \frac{\mathbf{J}_r}{j} \equiv \frac{1}{j}(J_{x_r},J_{y_r},J_{z_r}) \tag{22}$$

for $r=1,2$. We can now write the full Heisenberg equations of motion for these rescaled angular momenta. For example, Eq. (21) becomes

$$\begin{aligned} X_1' = {} & \frac{1}{2}(Z_1+iY_1)\exp\left[ik\left(-X_1+\frac{1}{2j}\right)\right]\otimes\exp(-ik\varepsilon Y_2) \\ & +\frac{1}{2}(Z_1-iY_1)\exp\left[-ik\left(-X_1+\frac{1}{2j}\right)\right]\otimes\exp(ik\varepsilon Y_2), \end{aligned} \tag{23}$$

and similar equations are obtained for the other five angular momentum operators.

To determine the classical equations of motion corresponding to the Heisenberg equations of motion such as Eq. (23) above, we must take the limit $j\to\infty$. To see this, consider the angular momentum commutation relations once more. In their rescaled form they become, for example, $[X_r,Y_r]=iZ_r/j$ for $r=1,2$. So, in the limit of $j\to\infty$ we can easily see that the rescaled angular momentum variable operators will commute and become c-number variables. Their stroboscopic time evolution in this situation will therefore be given by the Heisenberg picture equations in the large-j limit. If we first define

$$\Xi_1 := k(X_1+\varepsilon Y_2), \tag{24}$$

$$\Xi_2 := k(X_2+\varepsilon Y_1), \tag{25}$$

then we find

$$X_1' = Z_1\cos(\Xi_1)+Y_1\sin(\Xi_1), \tag{26}$$

$$Y_1' = -Z_1\sin(\Xi_1)+Y_1\cos(\Xi_1), \tag{27}$$

$$Z_1' = -X_1, \tag{28}$$

$$X_2' = Z_2\cos(\Xi_2)+Y_2\sin(\Xi_2), \tag{29}$$

$$Y_2' = -Z_2\sin(\Xi_2)+Y_2\cos(\Xi_2), \tag{30}$$

$$Z_2' = -X_2, \tag{31}$$

as our classical map. We therefore see that not only do the rescaled angular momentum variables become *c*-number variables as $j\to\infty$, but in this limit each $\mathbf{X}_r$, $r=1,2$, is also forced to lie on the unit sphere, i.e., $\mathbf{X}_r^2=1, r=1,2$.

In the limit of negligible coupling between the tops, i.e., as $\varepsilon\to 0$, we can see that $\Xi_r\to kX_r$, $r=1,2$. The classical equations of motion for our system then decouple into the equations of motion for two single, unperturbed tops [4], as required. The classical equations of motion for one such uncoupled top can be written (dropping subscripts)

$$X'=Z\cos(kX)+Y\sin(kX),$$
$$Y'=-Z\sin(kX)+Y\cos(kX), \tag{32}$$
$$Z'=-X.$$

These classical equations have been studied in depth by Haake in [4] and D'Ariano *et al.* in [19]. The variables X,Y, and Z lie on the unit sphere, $X^2+Y^2+Z^2=1$, and this restriction renders the classical map two dimensional. This fact provides us with the opportunity to reparametrize it using only the two usual polar and azimuthal angles θ and ϕ, respectively, according to

$$X=\sin\theta\cos\phi,$$
$$Y=\sin\theta\sin\phi, \tag{33}$$
$$Z=\cos\theta.$$

Moreover, the coordinates $Z=\cos\theta$ and $\phi=\arctan(Y/X)$ are, in fact, canonical coordinates on the sphere [4], and the classical map of Eq. (32) is a *canonical transformation* with a unit Jacobian. The map of Eq. (32) is therefore area preserving, with the infinitesimal area element on the unit sphere being $dS=\sin\theta d\theta d\phi$.

The classical trajectories generated by Eq. (32) depend for their character on the twist parameter, *k*. When $k=0$ the map describes a perfectly regular rotation around the *Y* axis. Increasing *k*, however, sees the familiar KAM scenario [2,4,19] with an increase in the area of the sphere covered by chaotic trajectories until, at approximately $k=6$, no visible stable islands exist and most trajectories are chaotic. In this study we will be interested in a regime residing between these two extremes of regular and chaotic behavior. That is to say, we will choose $k=3$ and consider the effect of an unequivocally mixed phase space on the quantum dynamics.

In Fig. 1 we give the classical phase space plot of a kicked top when $k=3$. The parametrization by ϕ and θ is particularly convenient as a means to represent the surface of the unit sphere on a two-dimensional surface. There are prominent islands of stability in a chaotic sea, giving us a truly mixed phase space. Two areas will, however, be of particular interest to us in the following and are marked by a filled square and triangle. The first clearly resides in a stable island on the sphere. This island [4] surrounds a fixed point of the classical map given above and has coordinates $(\theta_r,\phi_r)=(2.25,0.63)$. The second, marked by the filled triangle, is, by contrast, in the chaotic sea and nowhere near a regular island. Its coordinates are $(\theta_c,\phi_c)=(0.89,0.63)$.

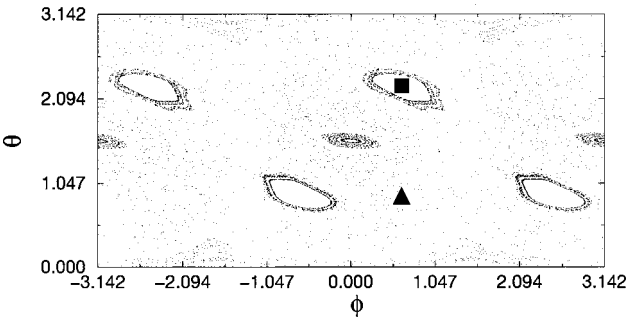

FIG. 1. Phase space plot for a single kicked top with $k=3$. The filled square and triangle mark areas of generically regular and chaotic behavior, respectively.

Of course, while phase space plots are useful for giving some indication of the qualitative features of the dynamics, they clearly do not give any quantitative information. In order to connect rates of quantum entanglement to measures of classical chaos, it is this information which is of interest. This is where the Lyapunov exponents become important and in the following we will show how to calculate the Lyapunov exponents of our coupled top system. First, though, we must describe the initial states used in both the quantum and classical numerical work that follows.

IV. INITIAL STATE

A. Quantum states

We wish to compare the classical and quantum evolutions of our system. For this purpose we require initial quantum states which best approximate an initial classical state on the sphere given by, for example, (θ_0,ϕ_0). If we recall that coherent states are the ''most classical'' states of the harmonic oscillator [26], then it will come as no surprise that coherent, minimum uncertainty states are suitable here too.

1. Directed angular momentum states

The coherent states we will choose to work with are the *directed angular momentum states* [4,19–21], denoted by $|\theta_0,\phi_0\rangle$. For a single top these states align the vector $\mathbf{J}_r$ along the direction from the origin to the point on the sphere parametrized by (θ_0,ϕ_0), i.e.,

$$\mathbf{n}_{\theta_0\phi_0}\cdot\mathbf{J}_r|\theta_0,\phi_0\rangle=j|\theta_0,\phi_0\rangle, \tag{34}$$

where $\mathbf{n}_{\theta_0\phi_0}$ is a unit vector pointing in the direction given by θ_0 and ϕ_0. These states can be conveniently generated using the eigenstate $|j,j\rangle$ ($|j\rangle$ in our notation) using a unitary rotation operator; in general,

$$|\theta_0,\phi_0\rangle=\exp\{i\theta_0(J_{x_1}\sin\phi_0-J_{y_1}\cos\phi_0)\}|j,j\rangle. \tag{35}$$

The sense in which the directed angular momentum states such a $|\theta_0,\phi_0\rangle$ ''best'' approximate the classical initial states (θ_0,ϕ_0) on the sphere can be seen from the following. First, the variance of the vector $\mathbf{J}_r$ in such a state is given by [20]

$$\frac{1}{j^2}\{\langle\theta_0,\phi_0|\mathbf{J}_r^2|\theta_0,\phi_0\rangle-\langle\theta_0,\phi_0|\mathbf{J}_r|\theta_0,\phi_0\rangle^2\}=\frac{1}{j}, \quad (36)$$

and obviously goes to 0 as we take the classical limit of $j\to\infty$. This is the minimum allowed by the angular momentum commutation relations. Second, it is shown by Schack *et al.* in Ref. [21] using the Husimi representation of the coherent state $|\theta_0,\phi_0\rangle$ that it is very small outside a region with a radius of about $2/\sqrt{j}$ radians around the center point (θ_0,ϕ_0) on the sphere. Explicitly, if α is the angle between the direction of the two points (θ_0,ϕ_0) and (θ_0',ϕ_0') on the sphere, then the square of the modulus of the overlap between the associated directed angular momentum states $|\theta_0,\phi_0\rangle$ and $|\theta_0',\phi_0'\rangle$ is given by [21]

$$Q(\alpha)\equiv|\langle\theta_0,\phi_0|\theta_0',\phi_0'\rangle|^2\approx\exp(-j\alpha^2/2) \quad (37)$$

for sufficiently large j. Clearly then, $Q(\alpha=2/\sqrt{j})=e^{-2}Q(0)$, a significant decrease. However, we can also look upon the function $Q(\alpha)$ as giving an as-yet-unnormalized Gaussian probability distribution for a deviation from the center in the direction (θ_0,ϕ_0). When normalized (denoted by the superscript N) this takes the form

$$Q^N(\alpha)=\frac{1}{\sigma\sqrt{2\pi}}\exp\left[-\frac{1}{2}\left(\frac{\alpha}{\sigma}\right)^2\right], \quad (38)$$

where σ is the standard deviation and is given by $\sigma=1/\sqrt{j}$. Clearly we have $Q^N(\alpha=2/\sqrt{j})=e^{-2}Q^N(0)$ here too.

In the following we will choose $j=80$, which gives an effective radius for our initial states of ≈ 0.22 radians. We have shown that this is sufficiently small to enable the quantum system to discern classical phase space structures such as those shown in Fig. 1.

However, we will require an explicit representation of the coherent states for calculations. As we will be working in the $|m_1\rangle$ basis for single top calculations and a tensor product of these for the coupled tops, we would like to express $|\theta_0,\phi_0\rangle$ as a superposition of these basis elements, $m_1=-j,\ldots,+j$. It is found [4]

$$\langle j,m_1|\theta_0,\phi_0\rangle=(1+\gamma\gamma^*)^{-j}\gamma^{j-m_1}\sqrt{\binom{2j}{j+m_1}}, \quad (39)$$

where $\gamma:=\exp(i\phi_0)\tan(\theta_0/2)$.

2. Initial tensor product state

For every initial state of the *coupled* top system, we will choose a direct product of two coherent states of the type described above. Explicitly,

$$|\psi(0)\rangle=|\theta_0^1,\phi_0^1\rangle\otimes|\theta_0^2,\phi_0^2\rangle, \quad (40)$$

with the evolution up to the (discrete) time n being given by

$$|\psi(n)\rangle=U_{\text{tops}}^n|\psi(0)\rangle, \quad (41)$$

where U_{tops} has been defined in Eq. (15). Because of the separable nature of Eq. (40), we may use Eq. (39) to write our initial state in the $|m_1,m_2\rangle$ representation discussed above. Explicitly,

$$\begin{aligned}|\psi(0)\rangle&=\sum_{m_1,m_2=-j}^{+j}\langle m_1,m_2|\psi(0)\rangle|m_1,m_2\rangle\\&=\sum_{m_1,m_2=-j}^{+j}\langle m_1|\theta_0^1,\phi_0^1\rangle\langle m_2|\theta_0^2,\phi_0^2\rangle|m_1,m_2\rangle,\end{aligned} \quad (42)$$

where, for example, each of $\langle m_r|\theta_0^r,\phi_0^r\rangle$, $r=1,2$, can be determined from Eq. (39).

B. Classical states

For the purpose of comparing the classical evolution of a *single* top to its quantum evolution, we must now construct initial classical *distributions* on the unit sphere analagous to the directed angular momentum states defined above. For example, in order to construct a classical state analagous to the state $|\theta_0,\phi_0\rangle$, we add to each of the angles θ_0 and ϕ_0 which define its center the *deviation* angles $\delta\theta_0$ and $\delta\phi_0$, respectively. These deviations are drawn from the normalized probability distribution defined in Eq. (38) above.

Furthermore, classical distributions analagous to the initial tensor product state of Eq. (40) above will be comprised of points of the form $(\theta_0^1+\delta\theta_0^1,\phi_0^1+\delta\phi_0^1,\theta_0^2+\delta\theta_0^2,\phi_0^2+\delta\phi_0^2)$ calculated in a similar manner.

V. NUMERICAL RESULTS

A. Iteration scheme

We can determine the matrix representation of an arbitrary state $|\psi(n)\rangle$ at time n from Eq. (15). We find

$$\begin{aligned}\langle s_1,s_2|\psi(n)\rangle&=\sum_{r_1,r_2=-j}^{+j}\langle s_1,s_2|U_\varepsilon^{12}|r_1,r_2\rangle\\&\quad\times\langle r_1,r_2|U^1U^2|\psi(n-1)\rangle\\&=\exp\left(-\frac{i}{j}k\varepsilon s_1s_2\right)\sum_{m_1,m_2=-j}^{+j}\{\langle s_1|U^1|m_1\rangle\\&\quad\times\langle s_2|U^2|m_2\rangle\langle m_1,m_2|\psi(n-1)\rangle\},\end{aligned} \quad (43)$$

where [17]

$$\begin{aligned}\langle s_1|U^1|m_1\rangle&=\exp\left(-\frac{ik}{2j}s_1^2\right)\langle s_1|U_f^1|m_1\rangle\\&=\exp\left(-\frac{ik}{2j}s_1^2\right)\frac{(-1)^{s_1-m_1}}{2^j}\\&\quad\times\binom{2j}{j-s_1}^{1/2}\binom{2j}{j+m_1}^{-1/2}\\&\quad\times\sum_k(-1)^k\binom{j-s_1}{k}\binom{j+s_1}{k+s_1-m_1}.\end{aligned} \quad (44)$$

The *reduced* density matrix $\rho_1(n)$ is determined from the entire, pure density matrix $\rho(n)$ using

$$\rho_1(n):=\text{Tr}_2[\rho(n)], \quad (45)$$

and its matrix elements are

$$\langle m_1|\rho_1(n)|n_1\rangle = \sum_{n_2=-j}^{+j} \langle m_1,n_2|\psi(n)\rangle\langle\psi(n)|n_1,n_2\rangle. \tag{46}$$

This enables us to calculate the level of entanglement between the coupled tops at time n on using the definition

$$E(n) := -\mathrm{Tr}_1[\rho_1(n)\ln\rho_1(n)], \tag{47}$$

where the set of eigenvalues $\{\lambda_{n_i}, i=-j, \ldots, +j\}$ is determined by first diagonalizing the $(2j+1)$-dimensional reduced density matrix at each time n. We then use

$$E(n) = -\sum_{i=-j}^{+j} \lambda_{n_i} \ln \lambda_{n_i}. \tag{48}$$

In the following we have chosen to use a value of $j=80$ at all times. The reasons for this choice are threefold. First, as stated in the preceding section, we have found $j=80$ to be perfectly sufficient to enable our chosen quantum initial states of Eq. (39) to distinguish between regular and chaotic areas on the classical unit sphere. Second, this value of j gave rise to reasonable running times, taking into consideration the fact that many runs were required to gather the data. Finally, such a relatively low value of j (see, for instance, the much larger values used in Refs. [4,17,20,21]) certainly means that we are far from the semiclassical regime. Any manifestations of chaos seen, therefore, are certainly examples of *quantum* chaos.

B. Linear increases in entanglement

We recall that in Fig. 1 for a single top we distinguished two initial points on the unit sphere. These points — a generically regular one marked by a square on that figure and a generically chaotic one marked by a triangle — we defined as $(\theta_r,\phi_r)=(2.25,0.63)$ and $(\theta_c,\phi_c)=(0.89,0.63)$, respectively. Keeping these states in mind, we now wish to investigate the rate at which three initial states of our quantized system become entangled. Thus, we choose three initial states where either (a) both states are initially regular, (b) one is chaotic and the other regular, or (c) both are chaotic. Using the notation of initial products of directed angular momentum states, see Eq. (40), we therefore choose either (a) $|\theta_r,\phi_r\rangle|\theta_r,\phi_r\rangle$, (b) $|\theta_c,\phi_c\rangle|\theta_r,\phi_r\rangle$, or (c) $|\theta_c,\phi_c\rangle|\theta_c,\phi_c\rangle$.

Using the iteration procedure described above, we now set $k=3$, fix our coupling constant ε, and calculate the entanglement, $E(t)$, for each of the three initial states. The results can be seen in Fig. 2: Initial product states where each subsystem is located in a classically chaotic area of that subsystem's phase space become entangled more quickly than those which have initially regularly located subsystems. In addition, the intermediate case of one subsystem being chaotic and the other regular gives rise to an entanglement rate which is also intermediate between these two extreme cases. The transition from situation (a) to situation (b) is shown in more detail in Fig. 3 and we find little change in the rates of entanglement. We shall elaborate upon these findings in the conclusions to follow.

The existence of this intermediate regime between the extremes of coupling two initially regular tops and two tops

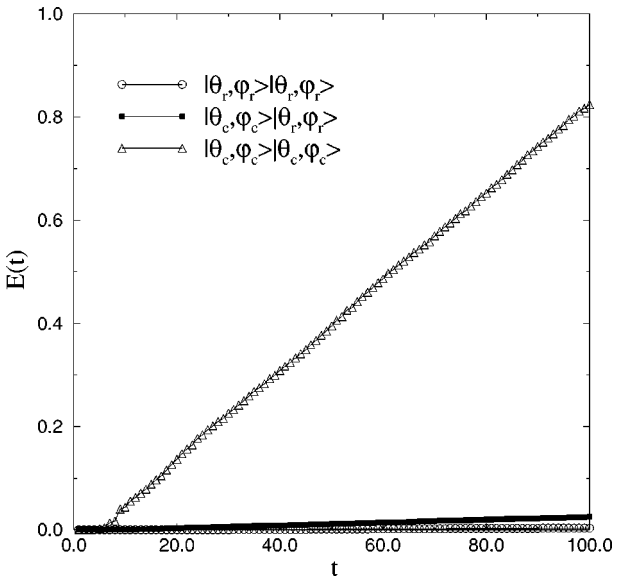

FIG. 2. An illustration of how entanglement rates differ as a result of the choice of the initial states, $|\psi(0)\rangle$, marked on the figure. Here we have chosen $\varepsilon=10^{-3}/3$ as our coupling strength.

that are initially chaotic is of special interest and we shall pursue this point henceforth. In fact, we will examine the consequences of interpolating smoothly between the two extreme situations. To do so classically we must first note that the initially regular and chaotic states marked in Fig. 3 differ only in their polar angle, θ. To go smoothly from regularity to chaos, therefore, involves nothing more than changing the initial polar angle from 2.25 to 0.89. Quantum mechanically, the interpolation from the entanglement behavior when the initial state is $|\theta_c,\phi_c\rangle|\theta_r,\phi_r\rangle$ to that when the initial state is $|\theta_c,\phi_c\rangle|\theta_c,\phi_c\rangle$ is achieved in a similar manner; we keep the initial state of the first top chaotic, i.e., $|\theta_c,\phi_c\rangle$, and begin with the initial state of the second top being regular, i.e., $|\theta_r,\phi_r\rangle$. We then calculate the rate of entanglement for initial states which differ only in the polar angle of the second

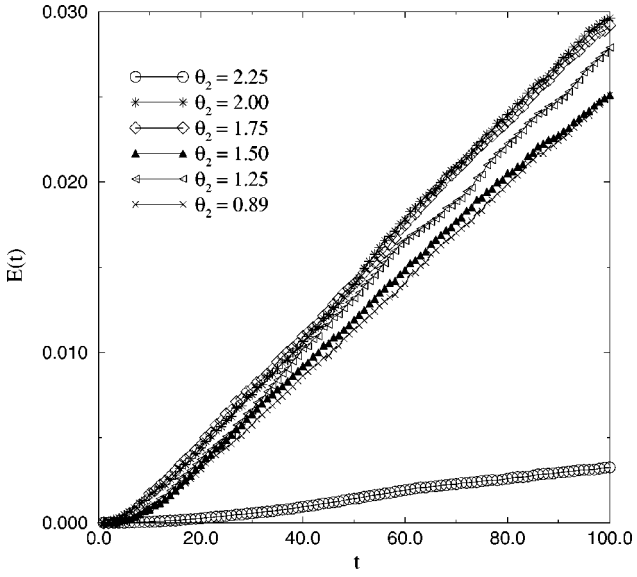

FIG. 3. Magnification of the regular-regular to chaotic-regular transition of Fig. 2.

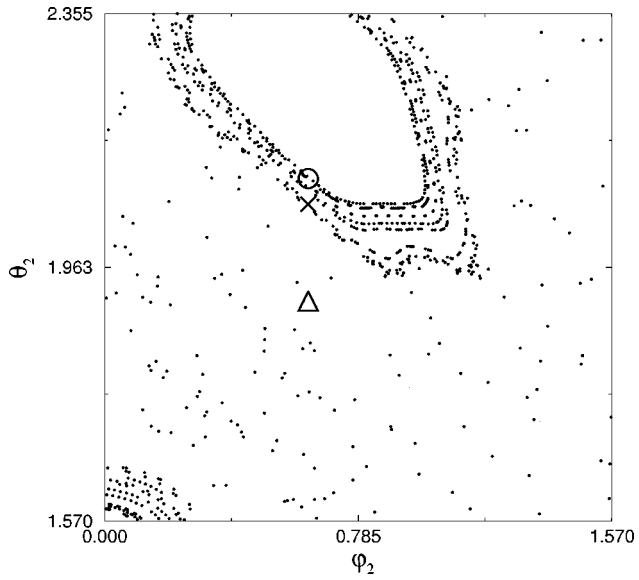

FIG. 4. A magnified section of Fig. 1, concentrating on the area around the stable island with the filled black square at its center in that figure. The open circle, cross, and triangle in this figure mark the center of three initial directed angular momentum states of the second top. The corresponding linear entanglement rates are shown in Fig. 5.

top, θ_2, with the range being from $\theta_2 = 2.25 \equiv \theta_r$ to $\theta_2 = 0.89 \equiv \theta_c$.

We can now confirm the linear nature of the entanglement increase with time by choosing three initial product states which differ only in their polar angle, θ_2. The centers of these initial states are plotted in Fig. 4 using the same symbols with which the associated increase of entanglement with time is marked in Fig. 5. To determine the linearity or otherwise, we have used linear regression to generate fits to the data, from $t = 30$ onwards, which we have also plotted in Fig. 5. The agreement is striking and the slopes so determined

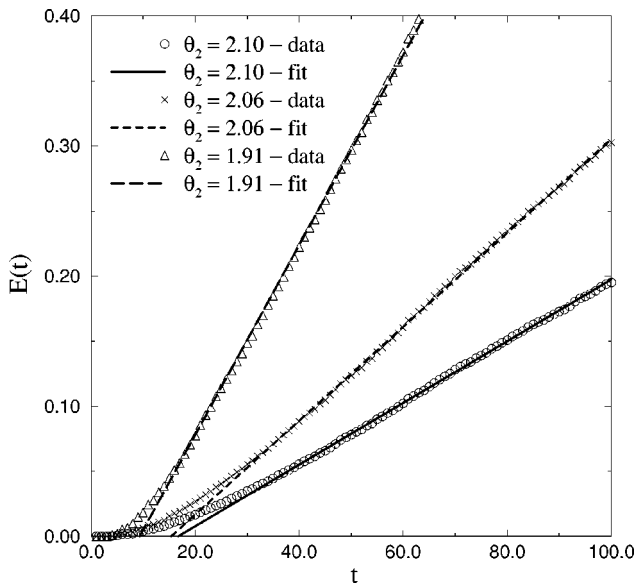

FIG. 5. Entanglement rates corresponding to the initial states of the second top which are marked by the same symbols in Fig. 4. Also shown are linear fits to the data from $t = 30$ onwards.

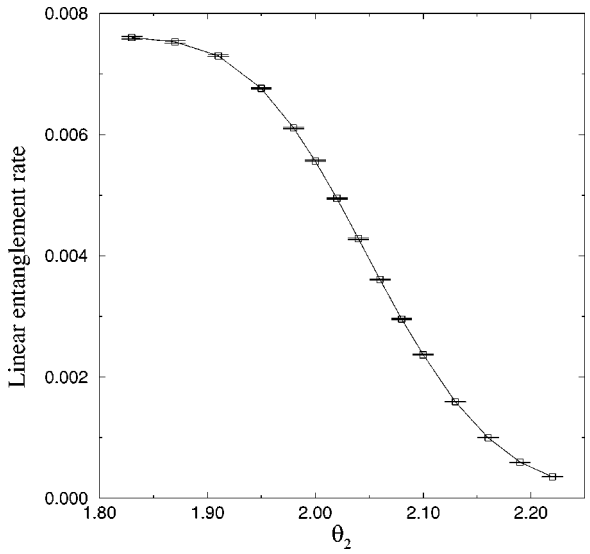

FIG. 6. Linear entanglement rate versus θ_2, the initial polar angle of the second kicked top. The tiny errors are a testament to the excellent linearity found.

can now be used to compare the quantum entanglement rates to measures of classical chaos determined from analagous initial classical distributions.

Our reason for choosing $t = 30$ is that in each of the three cases studied here it is larger than the steady-state time [6], τ_{ss}, at which the entropy of each state begins to increase linearly. In addition, it can be seen from Figs. 3 and 5 that the more chaotic the initial state of the second top is, the lower is τ_{ss}. This is consistent with the definition of τ_{ss} in Ref. [6].

C. Classical-quantum correspondence

We are now in a position to compare quantum with classical. First we determine the linear rates of entanglement increase for initial values of θ_2 on the unit sphere along the geodesic from $\theta_2 = 2.21$ to $\theta_2 = 1.83$. Very little change is noted for lower values since then the initial state will be contained entirely in the chaotic sea (see Fig. 6). We plot the results in Fig. 7. Both the smoothness and the nature of the transition — the errors being actually smaller than the square symbols used to plot the data points — provide yet more confirmation of the interpolation mentioned above.

A note of caution is necessary concerning the measures of classical chaos with which we will compare these quantum data. The phase space plots of Figs. 6 and 7 are useful and serve as guides to aid one in placing the *initial state*. This is so especially when the coupling is weak. However, they are, of course, plots of trajectories generated by the map associated with a *single* kicked top, Eq. (32). The quantum entanglement is generated by coupling the two tops and we must, therefore, consider the full classical equations of motion of our system, given by Eqs. (26)–(31), when comparing classical measures of chaos with quantum rates of entanglement. However, now a complication arises: the system of coupled kicked tops is confined to a four-dimensional subspace of six-dimensional Euclidean space, i.e., $S^2 \times S^2$, and this means that there will now be *two positive Lyapunov exponents* (and, of course, two negative exponents) associ-

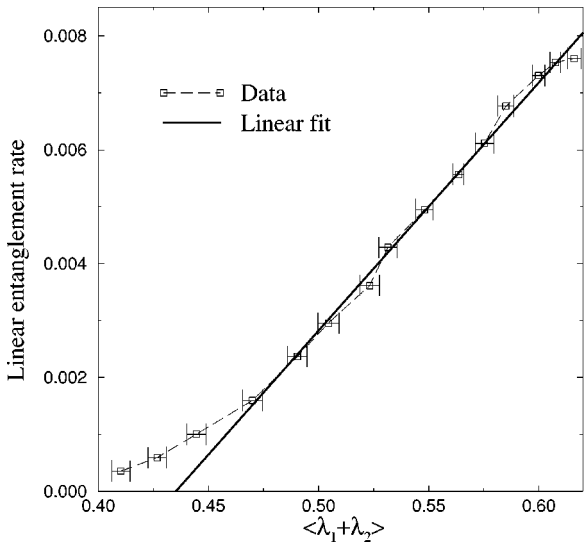

FIG. 7. Linear entanglement rate plotted against the averaged sum of the positive Lyapunov exponents for analagous initial classical distributions. Also plotted is a linear fit to the data away from the first three points.

ated with each initial condition $(X_1,Y_1,Z_1,X_2,Y_2,Z_2)$. The determination of both the positive Lyapunov exponents, λ_1 and λ_2 $(\lambda_1 \geqslant \lambda_2 \geqslant 0)$, is decidedly more tricky than the determination of the largest positive exponent only. We have used a method first proposed by Benettin *et al.* in Ref. [27] (and well explained in Chap. 5 of Ref. [28]) to do so.

Corresponding to each initial direct product state in the quantum analysis, the linear entanglement rates of which are plotted in Fig. 6, are two initial classical distributions of the type described in Sec. IV B. Sampling a point (X_1,Y_1,Z_1) from the distribution corresponding to the first top [always centered at (θ_c,ϕ_c) here] and a point (X_2,Y_2,Z_2) from the second [centered at (θ_2,ϕ_c) with θ_2 varying] gives rise to an initial classical state $(X_1,Y_1,Z_1,X_2,Y_2,Z_2)$ for which we can then determine the sum of the two positive Lyapunov exponents, $\lambda_1+\lambda_2$. We have carried out this procedure for 900 initial points in the distributions corresponding to each quantum initial state of Fig. 2.

In Fig. 7 we have plotted the linear entanglement rates of initial quantum product states versus the averaged (denoted by angular brackets) Lyapunov exponents of the associated initial classical distributions centerd at the same polar angle, θ_2. If we restrict our attention to those points with considerable overlaps with the chaotic sea (see Fig. 4), i.e., points with $\theta_2 \approx 2.13$ and smaller, we find that a linear fit to the data is quite a good one. Thus, our data lead us to propose the functional relationship

$$E(t) \approx (a_E \langle \lambda_1+\lambda_2 \rangle + b_E)t, \quad t > \tau_{ss}, \tag{49}$$

where τ_{ss} is the time at which the entanglement begins to increase linearly in time ($\tau_{ss} \leqslant 30$ here), and where a_E and b_E are functions of ε and j. Here, we note, $a_E \approx 0.044$ and $b_E \approx -0.019$. By differentiating both sides of Eq. (49) we find

$$\frac{dE}{dt} \approx a_E \langle \lambda_1+\lambda_2 \rangle + b_E, \quad t > \tau_{ss}. \tag{50}$$

D. Interpretation

How are we to interpret the result given by Eq. (49)? It says that after an initial time τ_{ss}, after which a steady state will have been established, a state of the coupled kicked top will become entangled at a rate which is constant in time. If the variables of the system are fixed, we have found that this rate is largely determined by the sum of the positive Lyapunov exponents when averaged over the classical distribution analagous to the initial quantum product state. Also, there is evidence to suggest that the rate depends linearly on this classical quantity.

If this interpretation is to be believed, then it leads one to propose an operational definition of chaos in the quantum regime. This is because a great advantage of choosing the quantum relative entropy as the measure of entanglement, Eq. (3), is the statistical interpretation afforded by it [23]. In this context we now interpret Eq. (49) in the following way: We consider the state of the system at any fixed time $t > \tau_{ss}$ and make a fixed number n of measurements on it. If all system variables such as ε, j, and k are held fixed, the probability, P_c, of confusing the state with a separable state decreases exponentially at a rate determined by the measure of classical chaos, $\langle \lambda_1+\lambda_2 \rangle$ defined above. Explicitly, we write

$$P_c = \exp(-nE(t)) = \exp(-nb_E t)\exp(-na_E \langle \lambda_1+\lambda_2 \rangle t). \tag{51}$$

VI. CONCLUSIONS

There is no classical behavior analagous to entanglement; it is unique to quantum mechanics. In this paper we have shown that this intrinsically quantum property exhibits a manifestation of classical chaos. In addition, the classical limit has not been taken in order to achieve this correspondence; the spin quantum number of each top has been kept to a relatively low value of $j=80$ throughout.

In the Introduction to this paper, one of our stated aims was to determine whether the phenomenon of a linear increase of entropy with time with a rate determined by measures of the underlying classical chaos, for an environment with a small number of degrees of freedom, was indeed a general one. We addressed this question by considering the entanglement rate of coupled kicked tops which, as we have seen, can be quantified by considering the von Neumann entropy of the reduced dynamics of a single top. By doing so, we have at least shown that coupling to a heat bath is not the *only* way of producing a linear entropy increase at a classically determined rate. However, as Fig. 7 shows, a certain threshold of chaos in each part of the coupled system must be crossed before Eq. (49) becomes valid. Just as temperature needs to be high enough in the Zurek and Paz approach for Eq. (49) to hold, so we require a certain level of chaos in the system for the entanglement to increase linearly with the (locally averaged) Kolmogorov-Sinai entropy.

This, then, provides yet more broad support for the original conjecture of Zurek and Paz made in Refs. [6,7], as generalized in Ref. [11], and the environmental decoherence approach to quantum chaos in general. In addition, because of the statistical interpretation of the measure of entanglement used here, we have been able to state the expected experi-

mental consequences of the entropic result of Eq. (49). In short, the more chaotic the system, the less likely one is to confuse it with a separable state, and this is the case to a greater degree as time passes.

At a *qualitative* level we believe that these results are related to some quantum features of the kicked top model noted by Haake *et al.* in Ref. [20]. The authors there considered the minimum number $N_{\min}$ of eigenvectors of the unitary single top evolution operator needed to exhaust the normalization of an arbitrary directed angular momentum state to within 1%. This, they have found, correlates very well with the largest Lyapunov exponent calculated for the point at the center of the coherent state. Indeed, for $k=3$ (see Fig. [6c] in Ref. [20]), $N_{\min}\approx 10$ at the center of a stable island, whereas $N_{\min}\approx 120$ elsewhere, i.e., in the chaotic sea. Initial direct products of such states would therefore require an increasing number of these eigenstates in an expansion in this basis as one or more of the initial subsystems is moved from a stable island into the chaotic sea. The subsequent introduction of the kick and interaction terms will then couple a greater number of eigenstates and a faster entanglement (loss of subsystem coherence) might reasonably be expected to occur.

However, our crucial finding is the simple functional form of Eq. (49). An intrinsically quantum-mechanical quantity has been shown to have a functional dependence upon a measure of the chaos exhibited by the classical analog of the initial quantum state, even when the reservoir is a finite chaotic system.

ACKNOWLEDGMENT

Paul A. Miller would like to thank the King's College London Association (KCLA) for financial support.

[1] G. Casati and B. V. Chirikov, *Quantum Chaos* (Cambridge University Press, Cambridge, 1995).
[2] L. E. Reichl, *The Transition to Chaos in Conservative Classical Systems: Quantum Manifestations* (Springer-Verlag, Berlin, 1992).
[3] *Chaos and Quantum Physics*, 1989 Les Houches Lectures, Session LII, edited by M. J. Giannoni, A. Voros, and J. Zinn-Justin (North Holland, Amsterdam, 1991).
[4] F. Haake, *Quantum Signatures of Chaos* (Springer-Verlag, New York, 1990).
[5] T. Dittrich and R. Graham, Ann. Phys. (N.Y.) **200**, 363 (1990).
[6] W. H. Zurek and J. P. Paz, Phys. Rev. Lett. **72**, 2508 (1994); G. Casati and B. V. Chirikov, *ibid.* **75**, 350 (1995); W. H. Zurek and J. P. Paz, *ibid.* **75**, 351 (1995).
[7] W. H. Zurek and J. P. Paz, Physica D **83**, 300 (1995).
[8] S. Habib, K. Shizume, and W. H. Zurek, Phys. Rev. Lett. **80**, 4361 (1998).
[9] W. H. Zurek, Phys. Scr. **T76**, 186 (1998).
[10] K. Shiokawa and B. L. Hu, Phys. Rev. E **52**, 2497 (1995).
[11] P. A. Miller and S. Sarkar, Nonlinearity **12**, 419 (1999).
[12] D. Giulini, E. Joos, C. Kiefer, J. Kupsch, I. O. Stamatescu, and H. D. Zeh, *Decoherence and the Appearance of a Classical World in Quantum Theory* (Springer-Verlag, Berlin, 1996), and references therein.
[13] R. Feynman and F. Vernon, Ann. Phys. (N.Y.) **24**, 118 (1963).
[14] A. O. Caldeira and A. J. Leggett, Physica A **121**, 587 (1983).
[15] P. A. Miller and S. Sarkar, Phys. Rev. E **58**, 4217 (1998).
[16] K. Furuya, M. C. Nemes, and G. Q. Pellegrino, Phys. Rev. Lett. **80**, 5524 (1998).
[17] A. Peres, in *Quantum Chaos*, edited by H. A. Cerdeira, R. Ramaswamy, M. C. Gutzwiller, and G. Casati (World Scientific, Singapore, 1991).
[18] A. Peres, *Quantum Theory: Concepts and Methods* (Kluwer, Dordrecht, 1993).
[19] G. M. D'Ariano, L. R. Evangelista, and M. Saraceno, Phys. Rev. A **45**, 3646 (1992).
[20] F. Haake, M. Kus, and R. Scharf, Z. Phys. B **65**, 381 (1987).
[21] R. Schack, G. M. D'Ariano, and C. M. Caves, Phys. Rev. E **50**, 972 (1994).
[22] R. Zarum and S. Sarkar (unpublished).
[23] V. Vedral and M. B. Plenio, Phys. Rev. A **57**, 1619 (1998).
[24] V. Vedral, M. B. Plenio, K. Jacobs, and P. L. Knight, Phys. Rev. A **56**, 4452 (1997).
[25] V. Vedral, M. B. Plenio, M. A. Rippin, and P. L. Knight, Phys. Rev. Lett. **78**, 2275 (1997).
[26] J. J. Sakurai, *Modern Quantum Mechanics* (Addison-Wesley, Reading, Massachusetts, 1994).
[27] G. Benettin, L. Galgani, A. Giorgilli, and J. M. Strelcyn, Meccanica **March** , 21 (1980).
[28] A. J. Lichtenberg and M. A. Lieberman, *Regular and Chaotic Motion* (Springer-Verlag, Berlin, 1992).